ANIMAL ROBOTS

Monopedal robot branch-to-branch leaping and landing inspired by squirrel balance control

Justin K. Yim[1]*†, Eric K. Wang[2]†, Sebastian D. Lee[3], Nathaniel H. Hunt[4], Robert J. Full[5], Ronald S. Fearing[6]

Locomotors traversing arboreal environments must often leap across large gaps to land on small-diameter supports. Balancing these dynamic landings is challenging because of high incident momentum, restricted foothold options, and reduced capacity to produce reaction torques on narrow supports. We hypothesized that leg length control to enhance branch reaction control authority would markedly expand the range of successful landing conditions, drawing on the same powerful leg actuation required for leaping. Exploring this balance strategy, the monopedal robot Salto-1P demonstrates branch-to-branch leaps, including some upright balanced landings, despite negligible grasping torque. We also compared this landing strategy with the landings of squirrels, which similarly lack the grip strength found in other arboreal species. We demonstrate that greater radial force control reduces the inertial body torque and/or grasping torque at the support required to balance a given landing. Adding simple radial force balance control strategies to conventional balance controllers greatly expands potential landing conditions, increasing the range of initial angular momentum that can be balanced by 230 and 470% across ranges of landing angles for low-order models of the robot and squirrel, respectively.

INTRODUCTION

Leaping and landing is often an essential behavior to negotiate gaps in natural and built environments. Some environments like tree branches have both large gaps that require large leaps and small-diameter footholds that must be accurately targeted. Leaping and landing on these kinds of "sparse" environments with both large gaps and small-diameter footholds is a great challenge because of the restricted control affordances of the terrain (Fig. 1A). Following such a leap to sparse footholds with a balanced, upright landing has not previously been demonstrated in a legged robot.

However, animals in nature, such as squirrels, are capable of leaping from branch to branch, providing inspiration for gap crossing (Fig. 1B) (*1*–*8*). Because of the challenges of negotiating sparse environments such as small-diameter branches that restrict footholds, squirrels often undershoot and overshoot landings. However, squirrels seldom fall because they have a remarkable fault-tolerant and fail-safe musculoskeletal system with mechanical computation built into the morphology (*6*).

Squirrels take gap-crossing ability one step further by producing upright, balanced landings, which provide a distinct advantage of being prepared for the next leap or even parkouring off the branch, demonstrating unparalleled agility (*6*, *8*). In addition to improved agility, upright locomotion above branch-like footholds is more efficient than inverted brachiation (*9*) and is applicable both in arboreal environments like trees and on continuous ground. Squirrels balance upright above branches despite lacking the long or prehensile grasping appendages of other arboreal species like primates, reducing the available torque they can exert on a foothold (*7*, *10*).

Here, we demonstrate a monopedal robot that can leap from branch to branch (Fig. 1C). See Movie 1 for a concise introduction. The greater than 80% success rate of no-fall landings resulted from high-performance branch balance and a very simple mechanical gripper system. Furthermore, the monopedal robot demonstrated branch-to-branch leaps with some upright balancing, achieving upright balance in 2 of 30 trials despite negligible grasping torque. Inspired by a squirrel's ability to balance upright above branches, we hypothesize an advancement in balance control. As observed in (*7*), squirrels modulate the force and torque they apply to a branch for balance depending on their landing initial conditions. Although applying torques to the branch to control balance angle is intuitive, the role of leg forces toward and away from the branch is less obvious. We hypothesized that the control of leg force and length to modulate the center of mass distance from the foothold could substantially expand the range of balanced landing conditions, drawing on the same powerful leg actuation required for leaping. We demonstrate that greater leg radial force control reduces the inertial body torque and/or grasping torque at the foothold required to balance a given landing. Adding radial force balance control to conventional balance controllers can greatly expand potential landing conditions for legged robots without requiring added actuation. In our balancing lander models (Fig. 1, D and E), radial force balance control increased the angular momentum that can be balanced by more than twofold across a range of landing angles.

Success in achieving an upright balanced landing is a subset of successful no-fall landing (Fig. 2). At touchdown, a catch is successful if grasping appendages engage with the branch and retain contact; a fall results if contact is lost. We present a simple passive gripper that enables branch catching while decoupling grasp force from leg extension and minimizing friction with the branch to enable balance control to follow. During the landing phase after a successful catch, the lander attempts to balance. Balance is successful if the lander moves from its landing initial conditions denoted with a subscript $_0$ to vertically align itself over the branch, avoiding overshooting in a swing-over or undershooting in a swing-under (*6*, *7*). We present balance control considering radial force to explain how the range of balanceable landing conditions can be

[1]Department of Mechanical Science and Engineering, University of Illinois Urbana-Champaign, Urbana, IL, USA. [2]Department of Mechanical Engineering, Massachusetts Institute of Technology, Cambridge, MA, USA. [3]Department of Mechanical Engineering, University of California, Berkeley, Berkeley, CA, USA. [4]Department of Biomechanics, University of Nebraska Omaha, Omaha, NE, USA. [5]Department of Integrative Biology, University of California, Berkeley, Berkeley, CA, USA. [6]Department of Electrical Engineering and Computer Sciences, University of California, Berkeley, Berkeley, CA, USA.
*Corresponding author. Email: jkyim@illinois.edu
†These authors contributed equally to this work.

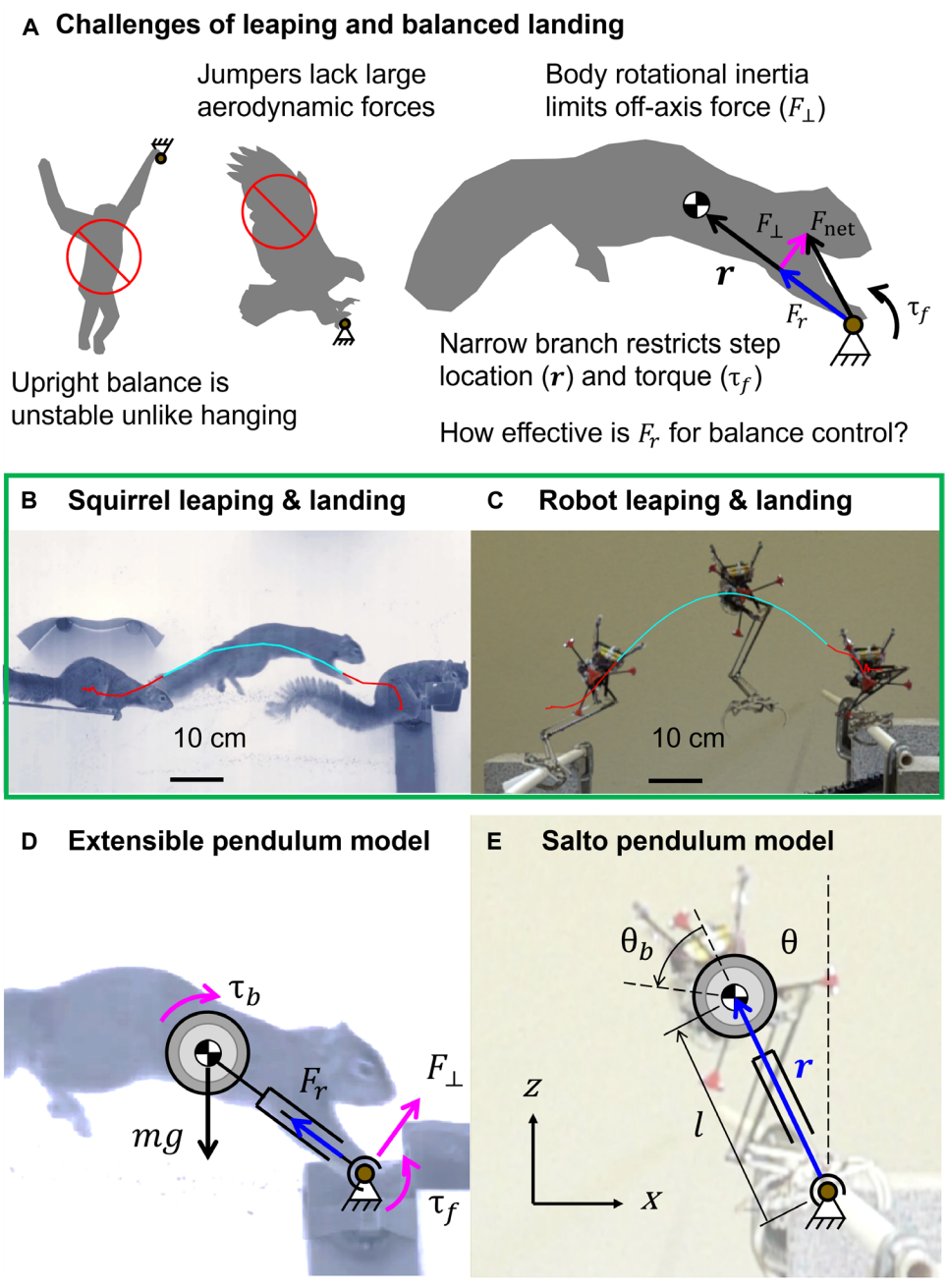

Fig. 1. Leaping and landing on sparse terrain. (**A**) Upright balanced landing after a leap is challenging because of restricted balance control affordances. Both squirrels (**B**) and the robot Salto (**C**) demonstrate branch-to-branch leaping and upright balanced landing despite small footholds and large gaps. Forces (**D**) and coordinates (**E**) for pendulum models of balancing lander dynamics in polar coordinates describe how interactions with the foothold (τ_f, F_r, and $F_\perp$) controlled by actuators (τ_f, τ_b, and F_r) affect CG motion (θ and r).

expanded. This balance behavior is particularly challenging, as described below.

RESULTS

Balance control

A landing balancer that does not fly and has no wings or rockets must control its locomotion using only its limited available foothold. We decompose legged locomotion into four control components (Fig. 1D), refocusing the decomposition of (*11*) to the task of branch landing control. This control involves either varying foot placement or components of the foothold reaction force. Foot placement refers to setting the initial value of vector $\boldsymbol{r}$ to be $\boldsymbol{r}_0$, defined as a vector from a point in the foot to the center of gravity (CG) immediately after landing. Varying components of the foothold reaction force includes modulating the radial force along vector $\boldsymbol{r}$, F_r; the perpendicular force to vector $\boldsymbol{r}$, $F_\perp$; or the torque about the foot contact, τ_f.

The most widespread robot locomotion controllers vary initial foot placement $\boldsymbol{r}_0$ (*12*, *13*) and foothold torque τ_f (*14*, *15*) to balance. Conventional controllers for multilegged robots use inputs equivalent to τ_f by applying different forces through multiple feet (*16*, *17*). However, on small-diameter branches, τ_f becomes restricted by the narrow moment arm, and $\boldsymbol{r}_0$ footstep-based control loses choices for where to put the foot on the initial landing and subsequent steps. In addition, large gaps produce challenging initial conditions for upright balance by necessitating leaps and corresponding high initial velocity at touchdown.

Balance control that accelerates or rotates inertial appendages effectively modulates $F_\perp$ (*18*–*20*). These controllers can balance on a knife edge or single point, but their control authority is limited by the finite angular momentum that their inertial appendages can store (*21*, *22*).

F_r is a particularly interesting control affordance for two reasons. First, its effectiveness is unchanged by foothold size. Second, locomotors capable of jumping generally already use very large radial forces to propel their jumps; controlling landing balance with F_r makes economical use of existing actuation. Many conventional hopping and running strategies, such as Raibert's seminal work (*12*), decouple controllers and neglect F_r's role in balance, but some walking control has made effective use of it (*23*–*26*). We focus on the effectiveness of F_r balance control in the unique context of upright balanced landing, derive a simple bang-bang control law (Materials and Methods), and compare the benefits of different landing force and torque components for balancing on widely separated small-diameter footholds.

In our considerations of balance, we focus on the planar motion and momentum of the lander relative to the foothold (Fig. 1, D and E). We can define the task of balance in terms of the lander's total linear and

Movie 1. Overview of branch-to-branch leaping and balanced landing. This video presents robotic branch-to-branch leaps and balanced landings, demonstrated by the monopedal robot Salto.

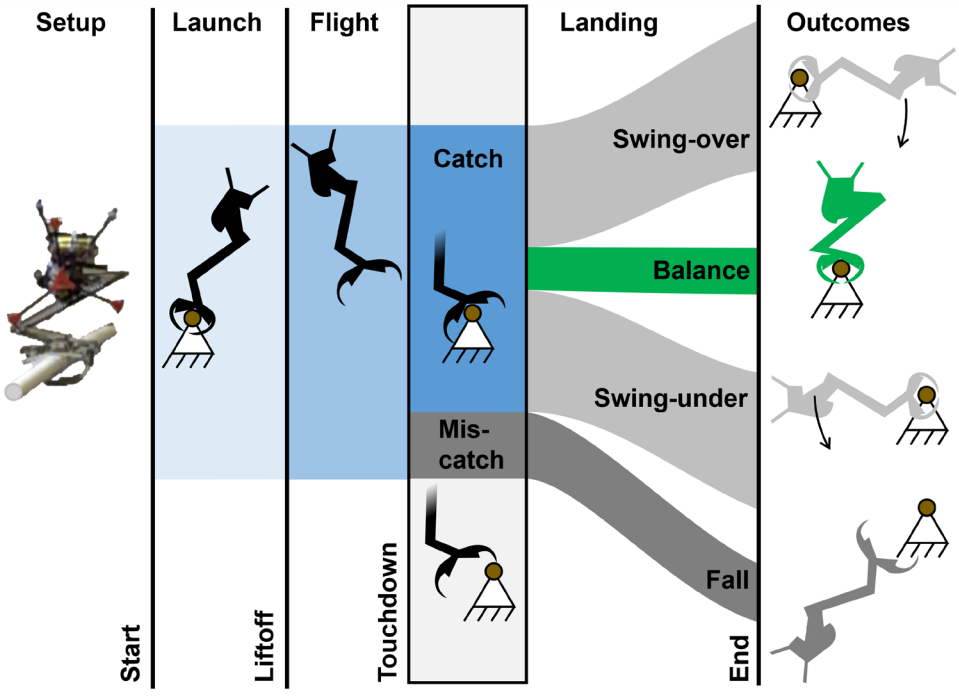

Fig. 2. Flow from initial state to potential leaping and landing outcomes. A balancing lander attempts first to catch the branch and avoid a fall, and then, if successful in catching, attempts to balance and avoid swinging over or swinging under. Catching requires accurately placing the gripper on the target branch, whereas balance requires agilely modulating angle and angular momentum to remain upright over the target branch.

angular momentum, so we parameterized the lander by its CG motion and the angular momentum about the CG. This can be captured in an extensible pendulum model with floating base coordinates of the CG relative to the foothold parameterized by polar tilt angle θ (the angle of $\boldsymbol{r}$ from the vertical), radial distance l (the magnitude of $\boldsymbol{r}$), and a body angle θ_b that captures angular momentum about the CG with an equivalent rotating body of appropriate moment of inertia (Fig. 1E).

The three virtual joints—θ, r, and θ_b—can be actuated by transforming the lander's internal forces into these joint coordinates with generalized forces termed τ_f, F_r, and τ_b, respectively (Fig. 1D). Although a squirrel's biomechanics intricately couple coordinated motion of its body, like spine bending and muscle activation, to produce forces that modulate CG motion, we adopt a simple parameterization of force that considers only a constant maximum value to represent the limited control authority of muscles or motors. Values for physical parameters and maximum combined force values (maximum radial force $F_{r_{max}}$ and maximum combined torque $\tau_{eff_{max}}$, described below) for squirrels and the robot Salto appear in Table 1. This simple parameterization is not a function of lander configuration and thus allows us to model squirrel or robot landing without detailed analysis of squirrel biomechanics.

We consider balance achieved when the CG is aligned on top of the foothold and the rotation of the CG about the foothold approaches zero. Specifically, this requires angular velocity $\dot{\theta} = 0$ and the CG to be aligned with the branch in one of two ways. Either angle $\theta = 0$, or if a lander can bring its CG close to the branch by wrapping its body around it, distance r must approach 0 while $|\theta| < \pi/2$. If r reaches zero, then the balancing lander is assumed to have collided inelastically with the branch to arrest its linear momentum in the radial direction. The CG dynamics are affected only by the foothold reaction forces and gravity given that squirrels and Salto cannot generate large aerodynamic forces. In the absence of aerodynamic forces, any lander's CG dynamics in the plane can be mapped to an extendable reaction-wheel inverted pendulum illustrated in Fig. 1 (D and E).

We further decompose the pendulum model's three control forces (F_r, τ_b, and τ_f) into two distinct groups on the basis of their action on the CG motion. Because the criteria for balance are based on the CG, any control strategy that achieves balance must shift the CG by modulating F_r and $F_\perp$. The extensible pendulum model actuates F_r directly, whereas τ_b and τ_f both modulate $F_\perp$ (see Supplementary Methods S1). Therefore, we can combine the action of τ_b and τ_f into one τ_{eff} acting at the foothold. τ_{eff} is the weighted sum of the two torques $\tau_{eff} = \tau_f + \alpha(-\tau_b)$ in which α is a scale factor between 1 and 0 to account for the finite moment of inertia of the body (see Supplementary Methods S2 for its derivation).

Table 1. List of parameters for squirrels and Salto. MoI, moment of inertia; DoF, degrees of freedom; –, not applicable

Symbol	Parameter	Units	Squirrels	Robot Salto
m	Mass	kg	0.829 ± 0.153	0.131
I_b	Body MoI estimate	kg•m^2	7×10^{-3}	7.3×10^{-5}
I_l	Leg MoI estimate	kg•m^2	Assumed negligible	1.3×10^{-4}
l_{min}	Minimum CG distance	cm	0	10
l_{max}	Maximum CG distance	cm	23.1 ± 1.7	21
$\tau_{eff_{max}}$*	Estimated max τ_{eff}	N•m/kg	0.5	0.18 to 0.21*
$F_{r_{max}}$	Estimated max F_r	Body weight	6	13†
DoF	Number of actuators	–	Many (>> 4)	4
–	Gripper compliance	–	Controlled variable stiffness	Passive rigid

*See Supplementary Methods S2 for derivation of Salto's effective torque τ_{eff} from τ_f and τ_b. †Despite Salto's high peak F_r, the robot's low-stiffness spring and leg mechanism nonlinearity produce slow F_r responsiveness given that the spring and mechanism were designed for leaping energetics and not landing balance.

Our extensible pendulum model contrasts with prior low-order models of walking (*24*–*28*) focusing on the task of jumping and landing on restricted footholds. We treat the actuators of the pendulum's joints as force sources and do not presume any intrinsic stiffness in any of the joints. Leaping to a branch and balancing upright are tasks related to the perching of flying robots previously demonstrated (*29*–*31*). Flying robots may lose control authority in a terminal stall just before touchdown, but jumping robots have no control authority over CG motion for the entire leap and lose negligible energy to drag, which necessitates particularly precise launch control and results in potentially high landing velocities. Furthermore, achieving upright balance like a squirrel—with low or no τ_f gripper torques and negligible aerodynamic deceleration—has not been demonstrated.

When landing on a small-diameter branch, a balancer uses only F_r and combined τ_{eff} to try to achieve balance because $\boldsymbol{r}_0$ is determined by flight kinematics and is no longer a control input (Fig. 3). The effect of each of these two balance control components has an intuitive interpretation. Positive τ_{eff} acts to slow rotation if the lander is overshooting, and negative τ_{eff} acts to speed up the rotation if the lander is undershooting. The effect of F_r can be thought of in two equivalent ways. First, applying F_r at a tilt angle θ produces a horizontal force of $F_x = -F_r \sin(\theta)$, which can be used to slow down the horizontal velocity of the balancing lander if it is swinging over or speed it up if it is swinging under. Second, positive F_r extends the distance r, increasing the balancing lander's moment of inertia about the foothold and reducing its angular velocity if the balancing lander is swinging over, with negative F_r producing the opposite effect. With this insight, the bang-bang controller illustrated in Fig. 3 chooses the sign of F_r and τ_{eff} on the basis of whether the lander is on a trajectory to swing over or swing under, denoted by a variable ε that is positive when swinging over and negative when swinging under. Measurements of squirrels' landing forces and torques show similar relationships between landing conditions and variation in force and torque (*7*).

The robot Salto-1P serves as a reduced-order platform to test the effectiveness of leg extension balance because of its close match to the extensible pendulum model of CG dynamics with a long straight-line leg and reaction wheel, near-squirrel scale, and high-performance jumping and precise control (*32*–*34*). To determine the effect of radial force control on the range of balanceable landing conditions for squirrels and Salto, we applied two extensible pendulum models illustrated in Fig. 1 (D and E). For the squirrels, we used the simple extensible pendulum model and bang-bang controller described above.

Salto, as an engineered system, can be precisely calibrated to produce a more detailed model, which we call the Salto pendulum model, with three modifications. First, a body with nonzero moment of inertia and CG location shared with the original body is inserted between the θ_b revolute joint and r prismatic joint. This body corresponds to Salto's chassis, whereas the original body now corresponds to Salto's reaction wheel. Second, τ_b follows a dc electric motor model. Third, the F_r dynamics are dictated by a series-elastic actuator model. Because the leg's series-elastic spring stiffness is low, the actuator's response is slow, and we replace a direct F_r command with a desired length, l_{des}, as described in Materials and Methods. Salto has two small aerodynamic thrusters that are used only to isolate its motion to the sagittal plane the way a boom mount would. They have minimal impact on in-plane dynamics of leaping and balancing, producing a maximum net force less than 15% of the total body weight and acting only perpendicular to the sagittal plane (see fig. S1). Because radial force can reach the upright balanced condition but cannot stabilize it, in experiments, Salto uses radial force balance control during the initial landing balance and uses conventional reaction wheel-based balance once it is upright near balance.

Robot leaping and landing experiments

Within 30 trials, Salto achieved 25 catches and 5 miscatch failures; landing catch kinematic conditions are plotted in Fig. 4. We developed Salto's lightweight caging gripper to capture the branch with negligible τ_f. We define two quantities, θ_v and d_v, to characterize the angle and lateral distance, respectively, from the branch to the incoming velocity v at the instant of touchdown. These two variables describe the kinematics of landing branch capture, but complicated branch impact behaviors mean that they are far from sufficient to entirely characterize capture success, as described in Discussion.

Salto executed two successful balanced landings in branch-to-branch leaping on a narrow support of 30 trials. The second of these two trials, trial 13, is shown in Fig. 5. We isolated F_r by exclusively using it and disabling Salto's reaction wheel during the first and

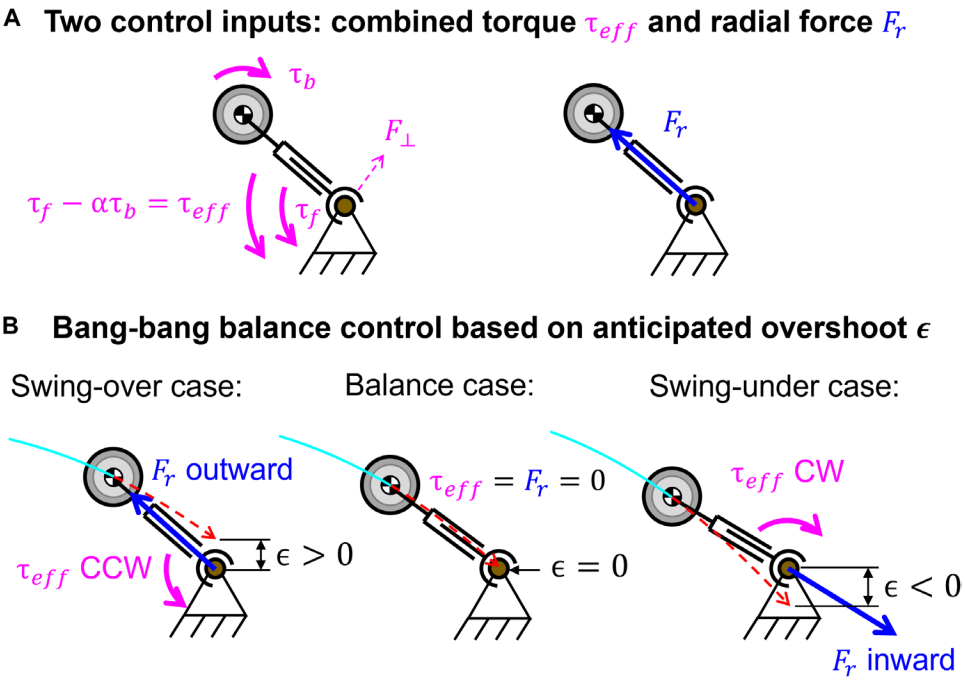

Fig. 3. Bang-bang balance control modulates F_r and τ_{eff} to balance. (**A**) F_r is actuated by the powerful muscles or motors that drive leaping, and τ_{eff} is a weighted combination of the actuated foot torque τ_f and body torque τ_b, which together generate a branch reaction force $F_\perp$ perpendicular to the leg axis. (**B**) The sign of the controlled force and torque depend on the anticipated overshoot ϵ of the CG trajectory over or under the branch to drive the CG to zero angular momentum about the branch.

most critical phase of the landing. Salto's onboard estimation detected touchdown 0.04 s after true touchdown and activated landing balance control at that time. Touchdown detection measured deflection of the leg's series-elastic spring and determined that touchdown had occurred only after the spring deflected past a threshold, which was chosen to avoid erroneous early touchdown detection as the foot oscillated in the air. Salto's F_r control kept the robot within the balanceable region of the reaction wheel acting alone (τ_{eff} strategy), and the reaction wheel finished the maneuver, settling to and remaining within ±10° of vertical after 0.22 s. Although the angular velocity varied as the robot bounced after its leg retracted to the bottom limit, it too remained near zero after 0.4 s.

Catching analysis

Leaping to and balancing on widely spaced, small-diameter footholds require accuracy and control. Unlike brachiating robots without an aerial phase (*35*) or perching flying robots (*29*–*31*, *36*–*38*), no control authority is available to adjust a jumper's CG trajectory just before touchdown. Although perches from winged flight frequently reduce speed to the point of stall (*30*, *36*, *37*), a leaping lander must handle the large incoming ballistic velocity, challenging both catch and subsequent landing. Catching a branch at speeds from 1 to 3 m/s was demonstrated by using high-friction soft pads or latching onto surface asperities (*29*–*31*), but this support torque-based τ_{eff} strategy becomes increasingly limited with diminishing branch radius. As opposed to releasing stored energy to produce grasping force (*30*, *31*), our gripper merely relies on a geometric cage to catch the branch, controlling balance with the radial force controller because our gripper decouples gripper engagement and friction from radial extension of the leg within a large range of lengths.

We model the gripper's geometry as an inverted "v," shown in Fig. 4A. If the branch is unable to physically contact the trigger linkage—a pair of linkages that transfer impact energy into the caging mechanism—the gripper will fail to grasp the branch. Each segment of this v is constructed by connecting a virtual line segment from the center of the gripper to the outside edges of the assembly that holds the trigger linkage. Illustrated in Fig. 4B, a gray bounded polytope can be constructed by varying θ_v and d_v along the geometric limits of the gripper, such that, outside this region, the branch is physically obstructed by other gripper features before it can contact the trigger linkage. Four cartoons demonstrate these geometric limits as θ_v is varied between its maximum and minimum limits while d_v is held constant, and d_v is varied between its maximum and minimum limits while θ_v is held constant. Each of the experimental trials is plotted at the moment of impact, with each "x" representing a failure to achieve a caging grasp and each "o" representing a catch—a successful caging grasp independent of balance.

Ninety percent of touchdowns, containing both successes and failures, lay within an SD of the polytope, demonstrating that the gripper's range of landing conditions is large enough and the launch accuracy is tight enough to reliably catch the target. However, the complicated interface of the gripper and branch provides many interactions that may have disrupted the 5 of 30 miscatch failures despite their placement around the gripper polytope. Out-of-plane deviation such as roll deflection (rotation about the x axis) could have caused the gripper roll bars to contact the branch before the gripper trigger linkage and foul its closing, or unpredictable rigid impact bounces may have placed the branch in an undesirable location (see Supplementary Methods S3 for discussion of disturbances and uncertainty). Compared with the highly actuated and compliant limbs of squirrels, Salto's unactuated and rigid gripper affords much less adaptability. Because of the focus on landing behavior, gripper interaction analysis is outside the scope of this work. Gripper design focused on enabling sufficiently reliable branch release and capture with low friction and low mass, and in this it succeeded.

Balanced landing control actuation space

Our experimental results demonstrate that a branch-to-branch leaping robot using radial force control can reach upright balance, but squirrels demonstrate unmatched robust upright balanced landings. In the following discussions, we analyze models of squirrels and robots to understand relationships among control strategies, physical parameters, and ability to balance. Both the simpler squirrel extensible pendulum model and more finely tuned Salto extensible pendulum model predict that radial force control substantially reduces the torque required to achieve an upright balanced landing (Fig. 6,

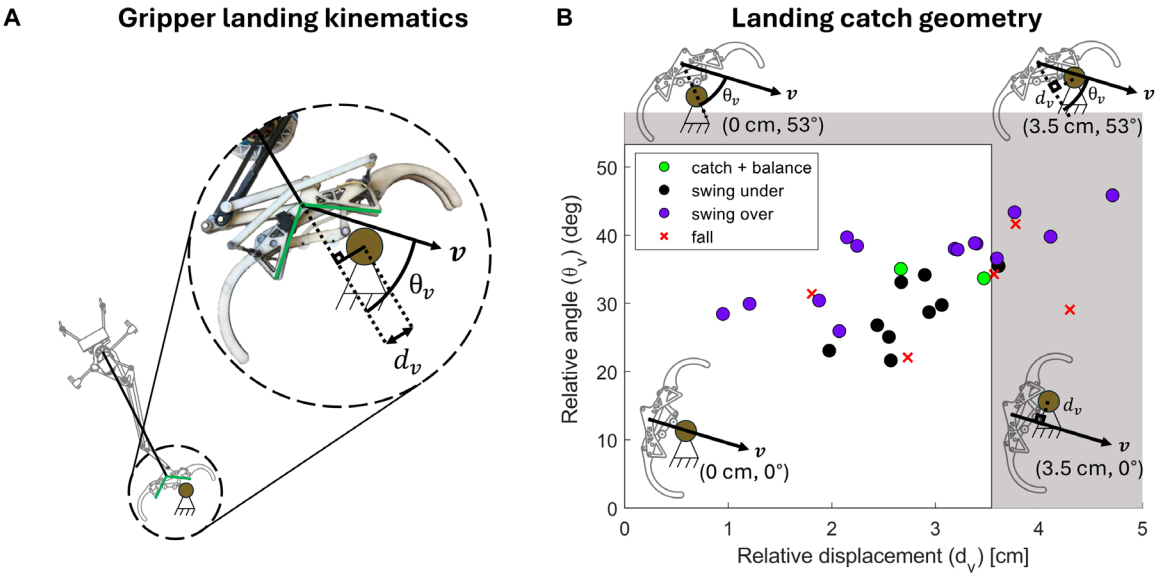

Fig. 4. Landing catch kinematics. (**A**) Relative gripper coordinates describing the configuration at impact are parameterized by displacement of the gripper relative to the branch d_v and angle of the gripper relative to the impact velocity vector θ_v. (**B**) Relative gripper coordinates at impact for Salto's 30 leaping and catching trials. Each point has a measurement uncertainty SD of 5 mm in d_v and 0.2° in θ_v based on motion capture precision and timing and robot mechanism uncertainty. White area shows that 90% of touchdowns lie within the SD of the polytope.

A and B) and expands the space of possible landing initial conditions from which balance can be reached (Fig. 6, C and D).

Extensible pendulum model simulations compare the balance capabilities of three control strategies: torque control only, radial force control only, and simultaneous torque and radial force control. We predict the range of control effort that can balance a particular initial condition and the range of initial conditions that a particular control effort can balance in Fig. 6. The landing actuation space is the combination of maximum F_r and maximum τ_{eff} that a balancing lander can use, represented by the orange boxes in Fig. 6 (A and B). Because Salto and squirrels on a narrow branch have the same set of reaction forces available, the extensible pendulum models described above capture CG dynamics, and the actuation space enables direct comparison with the following nondimensionalization.

For the squirrels, we set the body weight and length–normalized torque limit to be $\tau_{eff_{max}} = 20\%$ of body weight times radial length and the body weight–normalized radial force limit $F_{r_{max}} = 6$ times body weight on the basis of the largest branch torques τ_f and net reaction forces $|F_r + F_\perp|$ exerted by squirrels landing on an instrumented beam in (*7*). For the Salto extensible pendulum model, force and torque limits were calculated from physical parameters (see Supplementary Methods S2) to be $\tau_{eff_{max}} = 9.0\%$ of body weight times radial length and $F_{r_{max}} = 13$ times body weight, although Salto's slow F_r control response reduces the robot's ability to take advantage of its high peak force.

The exterior of the cross-hatched area delineates the minimum combinations of force and torque sufficient to balance from a particular initial condition. The initial conditions for representative squirrel trial 30 and robot trial 13 illustrated in Fig. 6 are given in table S1. Both representative trials began slightly overshooting (positive ε_0) and ended in successful balance. When attempting to balance a particular initial condition, we can choose how much τ_{eff} or F_r to use: Using more of one reduces how much is required from the other. As shown in Fig. 6A, the squirrel extensible pendulum model with a $F_{r_{max}}$ greater than 1.6 times body weight can balance the trial 30 initial condition with zero torque. Conversely, using a $\tau_{eff_{max}}$ control authority over 17% of body weight times maximum radial length can balance with no radial force control from this same initial condition.

Figure 6B shows that the Salto extensible pendulum model can also choose to use more τ_{eff} or more F_r to balance. However, the trial 13 initial condition is challenging enough that Salto needed nonzero amounts of both τ_{eff} and F_r to balance this landing.

Balanceable region

We show that a control strategy using both F_r control and τ_{eff} control together [the strategy labeled "3" in green in Fig. 6 (A and B)] expands the set of initial conditions that can be balanced compared with the strategy using τ_{eff} alone [the strategy labeled "1" in pink in Fig. 6 (A and B)] in sparse, small-diameter foothold environments. A controller's balanceable region is the set of initial conditions at touchdown from which the controller can drive the system to the balanced condition (related to the concepts of the balance state's capture region under the given controller and the balance backwards reachable set). The balanceable region is related to Roderick *et al.*'s (*29*) balance sufficiency region but with a particular focus on balance actuation parameters. In the following discussion, we show how adding F_r control to τ_{eff} control [green points in Fig. 6 (A and B)] expands the set of initial conditions that can be balanced compared with the use of τ_{eff} alone [pink location labeled 1 in Fig. 6 (A and B)] in sparse, small-diameter foothold environments. Touchdown initial conditions can be parameterized by three values: tilt angle θ_0, landing angular momentum L_0, and radial velocity $\dot{l}_0$ by assuming that touchdown always occurs when leg length is at maximum extension. Landing angular momentum L_0 is nondimensionalized by mr_{max}^2/T_c where

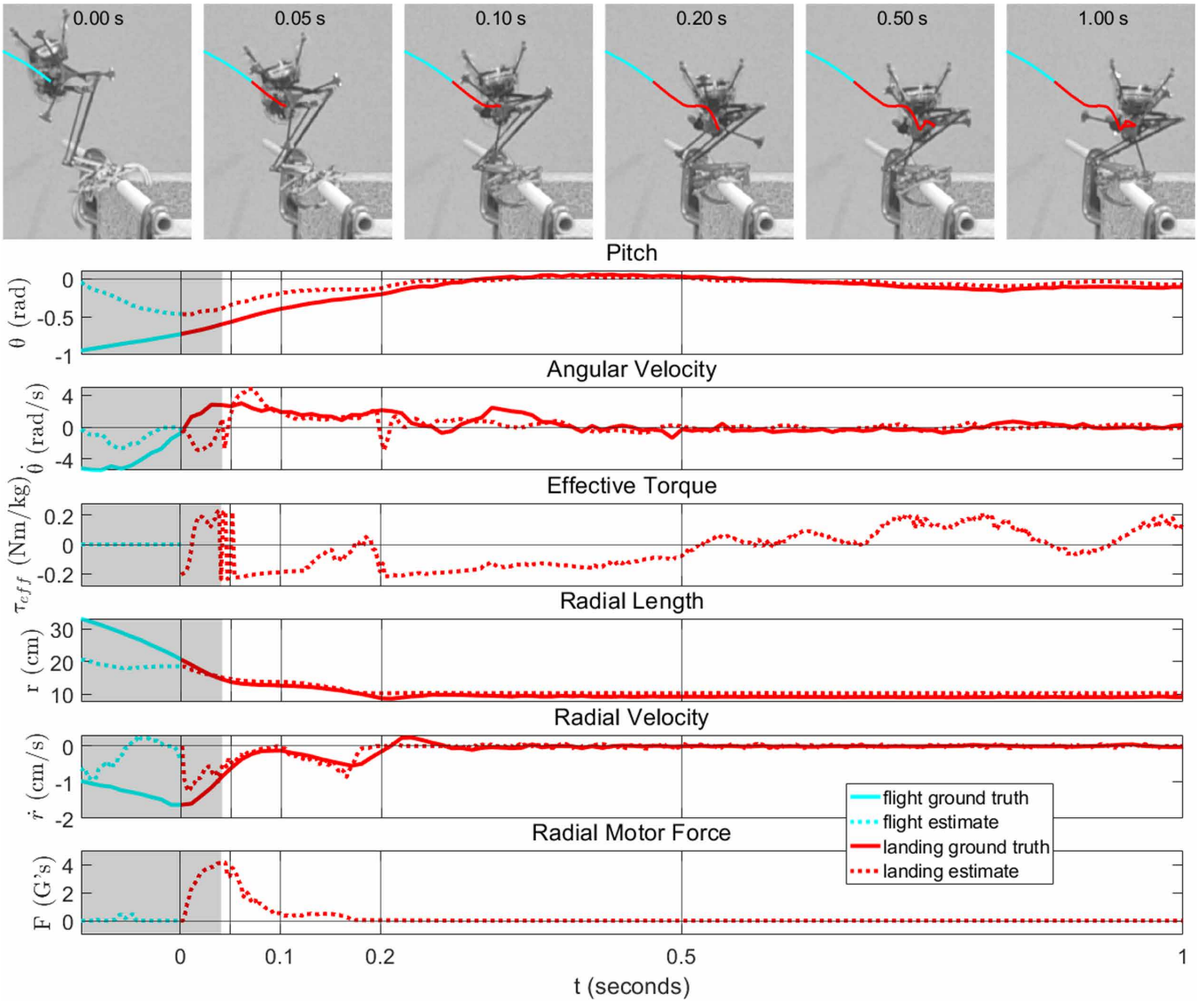

Fig. 5. Balanced landing. Salto achieves a balanced landing after leaping to a small-diameter foothold from a distance of 59 cm in experiment trial 13 (see Fig. 1C). Salto modulates first radial force (F) and then tail torque τ_b (a component of τ_{eff}) to balance, driving pitch, angular velocity, and radial velocity to zero. Touchdown occurs at $t = 0$ as determined from a high-speed video. Landing balance control activates at the end of the shaded region when Salto's onboard perception detects that it has landed. Ground truth states were postprocessed from motion capture, and state estimates used in real-time control were calculated from onboard sensing. Salto's thrusters confine its motion to the sagittal plane, applying forces only out of the plane and acting like an aerial version of a planarizing boom.

m is the mass, l_{max} is the maximum radial length, and T_c is the time constant of toppling [the pendulum time constant; see (*20*)].

$\dot{l}_0$ is nondimensionalized by l_{max}/T_c. θ_0 is already nondimensional. Assuming l_0 to be l_{max} at touchdown produces no loss of generality if touchdown impulse is negligible and τ_{eff} and F_r control is accurate because catching the branch later with a shorter length is equivalent to catching the branch at $l_0 = l_{max}$ and then applying zero force and torque until l reaches the shorter length.

Figure 6C shows that the addition of F_r greatly expands the squirrels' balanceable region from the pink area (τ_{eff} only) to the green area ($\tau_{eff} + F_r$), particularly at landing angular momenta that would have caused the squirrel to swing over on landing. For initial tilt angles of 30° and 90°, the combined $\tau_{eff} + F_r$ balanceable region is 470% larger than the torque-only τ_{eff} balanceable region, demonstrating a marked improvement in robustness to variation in swing-over angular momentum at landing.

In Salto, F_r produces a narrow balanceable region when used alone (Fig. 6D, blue), corroborated by the Salto's low experimental balance success rate. However, as in the squirrel extensible pendulum model, using torque and radial force control together, $\tau_{eff} + F_r$ (Fig. 6C, green), produces a much larger balanceable region than τ_{eff} alone. The green region has a 230% greater area than the pink region between tilt angles of 30° and 60°. F_r control provides greater balanceable region expansion at initial conditions with higher initial angular velocity and larger (more horizontal) tilt angles up to 60°. At tilt angles more horizontal than 60°, Salto does not retract its leg

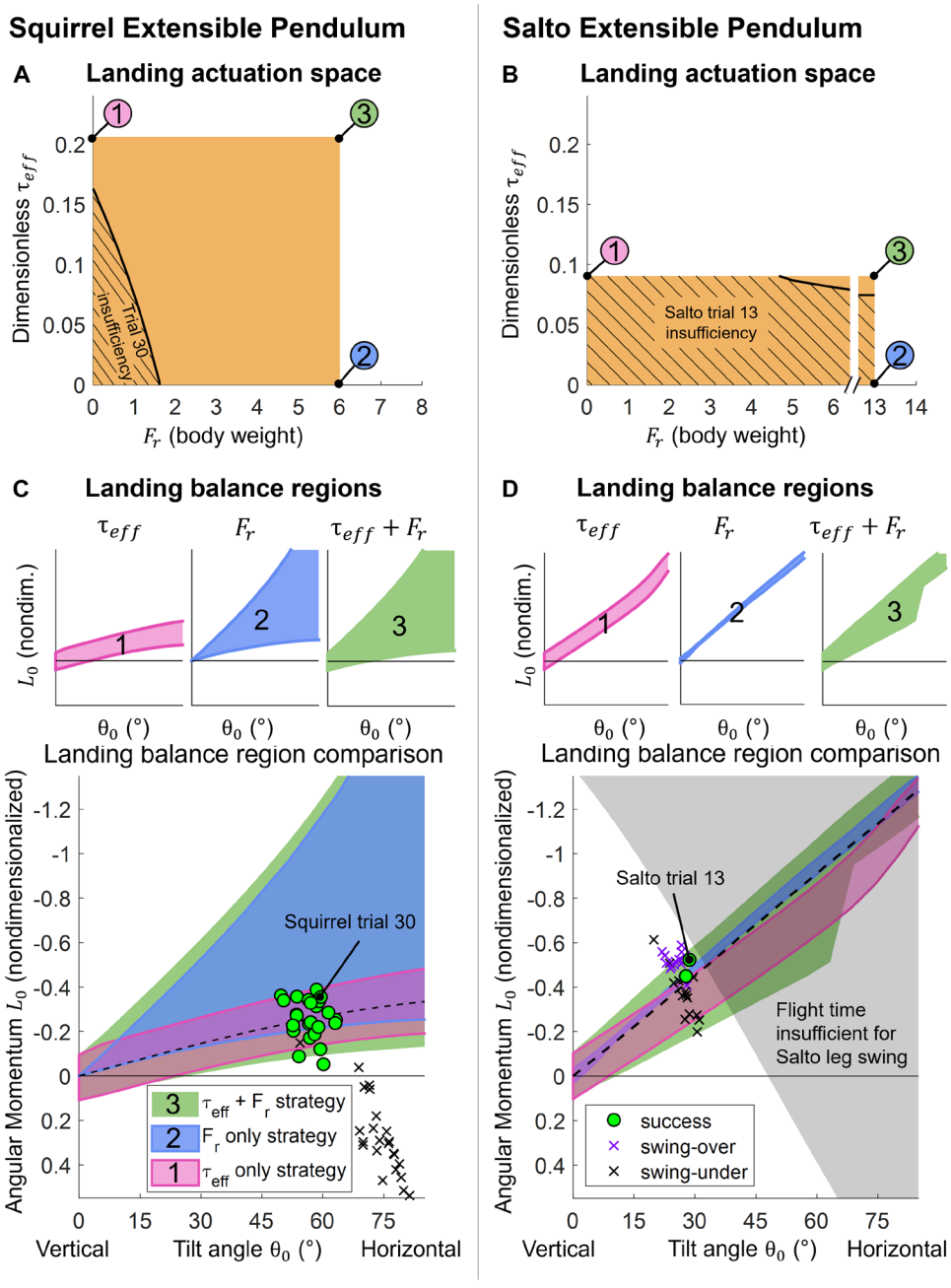

Fig. 6. Landing actuation space and balanceable regions. Combinations of F_r and τ_{eff} control authority that are sufficient for balancing an example experiment's initial condition for a squirrel (**A**) and robot Salto (**B**). Points inside the orange rectangle are within the actuation capabilities of the balancing lander, and points outside the hatched region provide sufficient control authority to balance the example initial condition. Balanceable regions are the set of initial conditions that can be balanced given landing actuation capability and strategy shown for squirrels (**C**) and robot Salto (**D**). The pink balanceable region uses only torque-based actuation, and blue uses only radial force, whereas green applies both torque and radial force to balance the widest range of initial conditions.

quickly enough under radial force balance control compared with simple energy removal, and thus it swings under the branch. The Salto extensible pendulum model's balanceable regions are substantially smaller than the squirrel extensible pendulum model's primarily because of Salto's lower τ_{eff}, inability to reduce r to zero, and the slow response of the leg extension controller tracking r_{des} (Eq. 4A in Materials and Methods). Our results build on previous investigations of F_r control (*23*–*26*) to show how effective it is in the high-speed, small-diameter foothold case of branch-to-branch leaping and landing. F_r control provides an unexpectedly large benefit in combination with τ_{eff} control, although when acting alone it cannot statically stabilize the stationary upright posture after reaching it.

Comparison of balanceable region models and robot experiment outcomes

To test the balanceable regions described by the squirrel extensible pendulum models, we overlaid the observed squirrel landing successes and failures from (*6*) in Fig. 6C on the balanceable regions predicted for strategies using only τ_{eff} (pink), only F_r (blue), and both $\tau_{eff} + F_r$ (green). Similarly, Fig. 6D plots the Salto extensible pendulum-predicted balanceable region. The balanceable region colors correspond to strategies in the same manner as the squirrel extensible pendulum model with the modification that in the Salto extensible pendulum model τ_{eff}-only strategy (pink), F_r simply aims to remove energy as in (*34*) without consideration for balance control.

The full predicted balanceable region for squirrels shown in green in Fig. 6C aligns with 46 of 48 squirrel experiment trials from the dataset of (*6*) (one false positive and one false negative). The study was approved by the University of California, Berkeley's Animal Care and Use Committee (AUP-2015-08-7830) and the California Department of Fish and Wildlife Nongame Wildlife Program. The agreement between the observations of squirrels and model predictions lends support to the squirrel extensible pendulum model's accuracy despite its simplicity (particularly lacking muscle dynamics or limb kinematics). Although most landing successes also lie within the balanceable region for a torque-only τ_{eff} strategy shown in pink in Fig. 6C, many lie close to its boundaries and would require torque very close to the maximum observed.

The Salto experiment's initial conditions overlaid in Fig. 6D agree closely with the predicted F_r-only balanceable region in blue that best matches the experimental controller. We initially hypothesized that F_r balance control would produce a large balanceable region and so selected this controller for all experiments run before the experimental apparatus became unavailable. Our analysis reveals

the expected large F_r balanceable region for the simpler squirrel extensible pendulum model but not for the Salto extensible pendulum model with more limited performance. The substantially larger $\tau_{eff} + F_r$ balanceable region compared with the radial force–only F_r region in Fig. 6D suggests that an experimental controller for Salto that combines radial force and effective torque $\tau_{eff} + F_r$ control would have achieved a higher success rate assuming accurate estimation and small disturbances. Despite these challenges, Salto demonstrated robotic branch-to-branch upright balanced landing and highlighted the importance of a balance control strategy, and not only a strong gripping torque, in producing this motion.

DISCUSSION

Morphology and control for landing balance

We identify four features important to upright balanced landing on small-diameter, distantly spaced branches: powerful and accurate jumping, shallow jump angles, short l_{min}, and combined torque and radial force control. First, powerful and accurate jumping enables a legged locomotor to cross a large gap to hit a small target and balance on it. Salto is a high-performance robot by jump power and jump accuracy (*32*, *34*); however, its design around a single powerful jumping leg is in tension with the second and fourth features described below: jump angle and force control speed.

Second, "shallower," more horizontal jumps that land at tilt angles farther from vertical are easier to balance. The balanceable region in Fig. 6 (C and D) is wider in this range of initial conditions (the right side at larger tilt angles). Here, lower peak landing forces and torques can be used when landings are further from the boundaries of the balanceable region. However, Salto is unable to reach this wider section of the balanceable region at horizontal initial tilt angles because, with one leg, Salto is subject to a minimum flight time constraint. Unlike the squirrels that leap from hind limbs and land initially with forelimbs, Salto has to reorient its single leg before touchdown and thus can spend no less than approximately 300 ms in the air, constraining it to operate below the shaded gray region in Fig. 6D and necessitating steeper, more vertical jumps.

Third, the ability to bring the CG close to the branch improves balance control. Whereas squirrels can wrap their torsos around a branch to bring their CGs close to its center, Salto's 10-cm l_{min} makes Salto's τ_{eff} control comparatively less effective at balancing. Salto must zero both $\dot{\theta}$ and θ simultaneously to achieve upright balance rather than zero only $\dot{\theta}$ as r approaches zero. Because Salto balances with a nonzero radial length, it uses a balance controller described in (*34*).

Fourth, as discussed in preceding sections, the combination of radial force control and torque control markedly increases balance capability and expands the range of landing initial conditions that can be balanced. However, radial force balance control necessitates relatively fast, responsive actuation. Salto's radial force actuation, which is optimized for generating high leaps, has a slow response time and thus cannot track rapidly changing desired forces. This relationship highlights a tradeoff between jumping and landing performance. As described in (*32*), series elasticity increases maximum jumping energy for small, length-constrained jumpers, enabling leaps between more widely separated branches. However, series elasticity is well known to reduce control bandwidth (*39*), hampering F_r balance control upon reaching the target branch. Parallel elasticity increases jump distance without reducing control bandwidth but could prevent the leg from retracting to short lengths, which also reduces balance control authority (*21*). Last, highly reliable mechanical structures with repeatable behaviors and highly reliable sensors with minimal noise or delay are musts for succeeding in this challenging branch-to-branch leaping and balanced landing behavior.

Incorporating all the features discussed above equips a locomotor to most reliably leap to and balance upright on small-diameter footholds. The interrelated contributions of l_{min} and the speed of F_r actuation are examined in more detail in Supplementary Methods S4 and fig. S4. These supplementary studies of the Salto pendulum model show that each of the morphological and control features contributes significantly to the size of balanceable region that a balancing lander can achieve.

Future directions

Future investigations can answer remaining questions about landing conditions, control, and correspondence to observations of animal behavior. The effects of collisions such as energy removal (despite conservation of momentum) may play an important role in balance. Extension of studies in arboreal animal leaping behaviors like those in (*7*) can further explore the role of pendulum balance control in arboreal animals' behaviors.

As noted in Salto's performance, a slow F_r response rate can limit balance performance, but the precise relationship in robots and corresponding time constants in animal landers are not well known. Reducing minimum radial length and increasing F_r bandwidth in future robot designs while considering the above tradeoffs could improve landing upright balance success rates.

MATERIALS AND METHODS

Gripper design

To better understand the role of grasping moments and alternative strategies in landing, we developed a nonactuated, lightweight caging gripper that deliberately minimizes gripping torque and friction at the contact interface expected on extremely small-diameter perches. This gripper was designed to meet several objectives: perching on top of a small-diameter foothold, supporting the robot swinging inverted beneath the foothold, automatically engaging when the robot lands from a wide range of approach angles in the sagittal plane, automatically disengaging when the robot leaps, and minimizing mass to avoid disrupting leaping and reorientation.

Previous robotic end effectors have mimicked specialized appendages and feet that arboreal species use to maintain a safe grasp while executing dynamic motions on sparsely distributed branches. Previous work has included grabbing objects in fly-by maneuvers (*40*, *41*) or engaging surfaces for leaping (*42*), climbing (*43*), and perching (*29*–*31*, *44*). However, in contrast with the presented gripper, these mechanisms rely on penetration or contact friction to impart moments onto the grasped body. The gripper intentionally produces a low-friction contact with the foothold, emulating the low τ_f available on small-diameter footholds.

The gripper is a six-bar Watt II linkage with a separate four-bar linkage attaching it to Salto-1P's leg, as shown in Fig. 7A. Like the Fin Ray effect grippers introduced in (*45*–*47*), this passive mechanism activates from an increase in normal contact force, but rather than using a soft truss system, it instead consists of a rigid toggle linkage design. A binary toggle link branch serves as the contact interface with the gripping surface and buckles when a normal force is

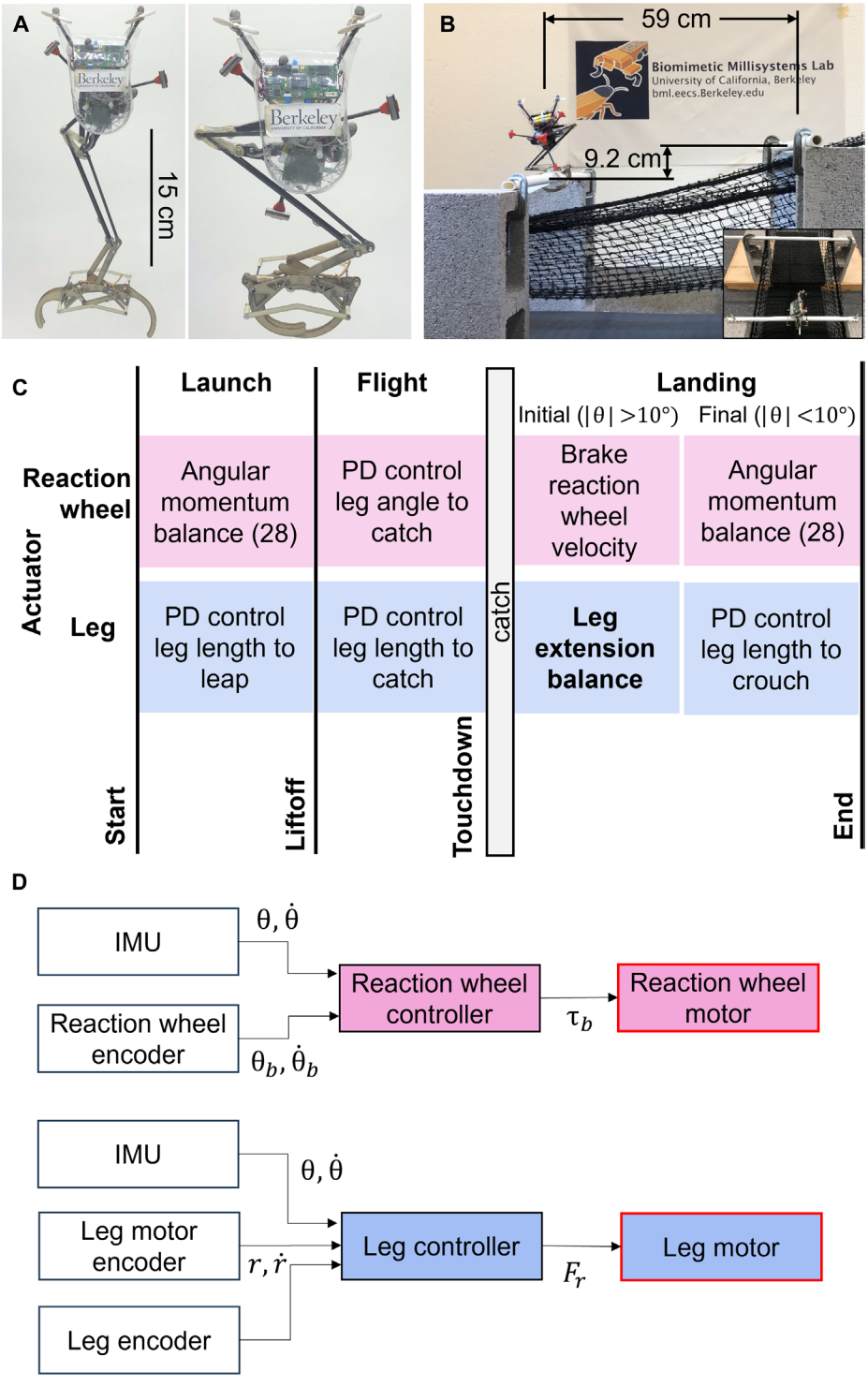

Fig. 7. Robot experimental setup. (**A**) Gripper mounted on Salto, in open (left) and closed (right) configurations. (**B**) Branch experimental setup with Salto perched on launch branch. (**C**) Control modes and (**D**) control block diagram for launch, flight, and landing phases used by the robot onboard control sequence.

applied. This buckling causes the binary link to rotate past its toggle position and invert, locking the mechanism. Two claw linkages are coupled so that their rotational motions are mirrored with the action of the toggle link. When an outward force is applied to the claws after the mechanism has locked, a high mechanical advantage from the toggle link results in little deformation. This allows the gripper to maintain a loose grip around the branch even when experiencing high outward forces. A lever attached to a separate four-bar linkage unlocks the toggle linkage when the leg extends past a predetermined distance, and when the gripper is open, this lever does not contact the six-bar linkage. This couples the motion of Salto-1P's leg to the disengagement of the gripper during its leaping phase and decouples the leg from gripper engagement during its landing phase.

Two wheels along the toggle linkage offer a rolling interface to minimize friction when the gripper rotates with respect to the branch. They also ensure that the point of rotation is located at the center of the branch. To constrain behavior to the modeled sagittal plane, two roll bars protruding from the planar surface of the gripper were designed to compensate for Salto-1P's weaker out-of-plane control authority in the roll direction. The planar linkage assembly was manufactured by laser cutting a composite of fiberglass and balsa wood, chosen for their high rigidity-to-weight ratio. Plastic dowels and carbon fiber rods were used for the axles, and the wheels were laser-cut from a $^{1}/_{16}$-inch (1.6-mm) Delrin sheet. The gripper along with Salto-1P's modified "tarsus" link (the final link of the robot's leg linkage) has a mass of 11.6 g in total.

Robot experimental setup

The experimental setup consisted of two doubly clamped $^{27}/_{32}$–inch (21-mm)–diameter polyvinyl chloride pipes that function as the starting and landing branches, suspended above a safety net, as shown in Fig. 7B, and separated with a gap distance of 59 cm and a vertical rise of 9.2 cm. Salto-1P begins every trial perched using balance control on the starting branch, whose side view and top view are shown in Fig. 7B. An OptiTrack motion capture system records orientation and positional data in the world frame at 100 Hz. On board the robot, control is executed at a frequency of 500 Hz, and logged data are transmitted to the ground station after each trial.

Robot CG position is measured in the sagittal plane from motion capture, and robot foot position is estimated using onboard encoder data coupled with the leg's kinematic linkage model. Pose is measured using motion capture because the onboard TDK InvenSense MPU-6000 IMU suffers from too much vibrational noise during landing because of a combination of high landing accelerations and

gripper movements. However, because the reflective markers are occluded from the vision system when the robot swings directly underneath the branch, we lose the inverted portion of the state trajectory during trials in which the robot undershoots or overshoots the balance condition.

We iteratively tuned launch parameters in physical experiments to find a solution that achieved appropriate conditions for landing. We then fixed all experiment parameters and ran 30 trials with identical parameters to evaluate performance and reliability of the launch and balanced landing behaviors.

The control and planning structure for each experimental trial is shown in Fig. 7 (C and D). In the launch phase, the selected launch parameters determine the commanded angular momentum trajectory and leap timing to bring the robot to its desired touchdown condition. For the aerial phase, a fixed landing angle and leg length were empirically chosen for all trials. Last, the robot attempts to either apply a swing up maneuver or balance control after touchdown depending on whether the angular position was within the torque balance region.

Balance control derivation

Assuming simple peak force limits apply to all foothold reaction force components, we derived a bang-bang controller to attempt to reach balance from landing initial conditions. Given that foothold diameters are small in sparse environments, we considered the choice of initial foot placement vector $\boldsymbol{r}_{t=0}$ to be restricted to essentially one point, leaving only τ_{eff} and F_r to control balance. For the squirrel extensible pendulum model, we consider balance to be successful if length r approaches zero while $|\theta| < \pi/2$ by assuming that this condition represents a collision with the branch with the CG near the foothold. Squirrels demonstrate such balanced landings in (*6*) by wrapping their torsos around the branch. Given this success condition, the bang-bang controller can act on the projected distance that the CG would pass above or below the branch under ballistic motion from its current state. This value ε is termed the "landing error" in (*6*), but we call it the "anticipated overshoot" because we consider this quantity as it varies during the landing motion for balance control

$$\varepsilon = r_z + \dot{r}_z \Delta t - \frac{g\Delta t^2}{2} \tag{1}$$

$$\Delta t = -\frac{r_x}{\dot{r}_x} \tag{2}$$

where Δt is the time until the balancer is vertically aligned with the foothold, r_x and r_z are the horizontal and vertical displacements of the CG from the foothold, and g is the acceleration due to gravity. The bang-bang controller force components can then be expressed as

$$\tau_{\text{eff}} = \tau_{\text{eff}_{\max}} \operatorname{sign}(\varepsilon) \tag{3A}$$

$$F_r = F_{r_{\max}} \operatorname{sign}(\varepsilon) \tag{3B}$$

where $\tau_{\text{eff}_{\max}}$ and $F_{r_{\max}}$ are the maximum effective torque and the radial force, and $\operatorname{sign}(\varepsilon)$ is 1 when ε is positive, −1 when it is negative, and 0 when it is 0. This control law is illustrated for different values of ε in Fig. 3. This bang-bang control is optimal for achieving balance from the widest range of landing conditions when ε is positive and is not optimal but still effective when ε is negative.

Because of the slow response of Salto's low-stiffness series-elastic leg actuator, the bang-bang F_r force controller that commands swift changes in output force was replaced with a smoother desired leg length command for robot experiments. The desired length r_{des} was chosen to be the length that achieves balance without torque τ_{eff} control. In this strategy, the force control in Eq. 3B is replaced with position control by setting desired length l_{des}

$$l_{\text{des}} = \left(-2mg^{1/2}\sin(\theta/2)/L\right)^{-2/3} \tag{4A}$$

$$L = mr^2\dot{\theta} \tag{4B}$$

Similarly, the bang-bang τ_{eff} torque controller is replaced by the reaction wheel balance control of (*34*) for Salto.

Supplementary Materials

The PDF file includes:

Methods S1 to S4
Figs. S1 to S4
Tables S1 and S2
Legends for movies S1 and S2
Reference (*48*)

Other Supplementary Material for this manuscript includes the following:

Movies S1 and S2
Data file S1

REFERENCES AND NOTES

1. M. Cartmill, "Pads and claws in arboreal locomotion" in *Primate Locomotion*, F. A. Jenkins Jr., Ed. (Elsevier, 1974), pp. 45–83.
2. C. H. Cannon, M. Leighton, Comparative locomotor ecology of gibbons and macaques: Selection of canopy elements for crossing gaps. *Am. J. Phys. Anthropol.* **93**, 505–524 (1994).
3. A. J. Channon, J. R. Usherwood, R. H. Crompton, M. M. Günther, E. E. Vereecke, The extraordinary athletic performance of leaping gibbons. *Biol. Lett.* **8**, 46–49 (2012).
4. M. Graham, J. J. Socha, Going the distance: The biomechanics of gap-crossing behaviors. *J. Exp. Zool. A: Ecol. Integr. Physiol.* **333**, 60–73 (2020).
5. F. Druelle, P. Aerts, J. C. B. Nagawolo, V. Narat, Impressive arboreal gap-crossing behaviors in wild bonobos, *Pan paniscus*. *Int. J. Primatol.* **41**, 129–140 (2020).
6. N. H. Hunt, J. Jinn, L. F. Jacobs, R. J. Full, Acrobatic squirrels learn to leap and land on tree branches without falling. *Science* **373**, 697–700 (2021).
7. S. D. Lee, S. Wang, E. K. Wang, J. K. Yim, N. H. Hunt, R. S. Fearing, H. S. Stuart, R. J. Full, Free-ranging squirrels achieve above-branch balanced landing with leg force and nonprehensile grasp torque. *J. Exp. Biol.* 10.1242/jeb.249934 (2025).
8. D. Youlatos, A. Samaras, Arboreal locomotor and postural behaviour of European red squirrels (*Sciurus vulgaris* L.) in northern Greece. *J. Ethol.* **29**, 235–242 (2010).
9. P. E. Parsons, R. C. Taylor, Energetics of brachiation versus walking: A comparison of a suspended and an inverted pendulum mechanism. *Physiol. Zool.* **50**, 182–188 (1977).
10. J. W. Young, B. A. Chadwell, Not all fine-branch locomotion is equal: Grasping morphology determines locomotor performance on narrow supports. *J. Hum. Evol.* **142**, 102767 (2020).
11. Y. Gong, J. W. Grizzle, Zero dynamics, pendulum models, and angular momentum in feedback control of bipedal locomotion. *J. Dyn. Syst. Meas. Control* **144**, 121006 (2022).
12. M. H. Raibert, B. H. Brown Jr., M. Chepponis, Experiments in balance with a 3D one-legged hopping machine. *Int. J. Robot. Res.* **3**, 75–92 (1984).
13. J. Pratt, J. Carff, S. Drakunov, A. Goswami, Capture point: A step toward humanoid push recovery, in *Proceedings of 2006 6th IEEE-RAS International Conference on Humanoid Robots* (IEEE, 2006), pp. 200–207.
14. M. Vukobratovic, D. Juricic, Contribution to the synthesis of biped gait. *IEEE Trans. Biomed. Eng.* **1**, 1–6 (1969).
15. M. Vukobratovic, B. A. Borovac, Zero-moment point – thirty five years of its life. *Int.J. Humanoids Robot.* **1**, 147–173 (2004).

16. R. B. McGhee, A. A. Frank, On the stability properties of quadruped creeping gaits. *Math. Biosci.* **3**, 331–351 (1968).
17. M. Neunert, M. Stäuble, M. Giftthaler, C. D. Bellicoso, J. Carius, C. Gehring, M. Hutter, J. Buchli, Whole-body nonlinear model predictive control through contacts for quadrupeds. *IEEE Robot. Autom. Lett.* **3**, 1458–1465 (2018).
18. J. Hauser, R. Murray, Nonlinear controllers for non-integrable systems: The Acrobot example, in *Proceedings of American Control Conference* (IEEE, 1990), pp. 669–671.
19. M. W. Spong, P. Corke, R. Lozano, Nonlinear control of the reaction wheel pendulum. *Automatica* **37**, 1845–1851 (2001).
20. R. Featherstone, A simple model of balancing in the plane and a simple preview balance controller. *Int. J. Robot. Res.* **36**, 1489–1507 (2017).
21. R. Featherstone, Quantitative measures of a robot's physical ability to balance. *Int. J. Robot. Res.* **35**, 1681–1696 (2016).
22. J. J. Driessen, A. E. Gkikakis, R. Featherstone, B. R. P. Singh, Experimental demonstration of high-performance robotics balancing, in *Proceedings of IEEE International Conference on Robotics and Automation* (IEEE, 2019), pp. 9459–9465.
23. B. J. van Hofslot, R. Griffin, S. Bertrand, J. Pratt, Balancing using vertical center-of-mass motion: A 2-D analysis from model to robot. *IEEE Robot. Autom. Lett.* **4**, 3247–3254 (2019).
24. T Koolen, M. Posa, R. Tedrake, Balance control using center of mass height variation: Limitations imposed by unilateral contact, in *Proceedings of 2016 IEEE-RAS International Conference on Humanoid Robots (Humanoids)* (IEEE, 2016), pp. 8–15.
25. S. Caron, Biped stabilization by linear feedback of the variable-height inverted pendulum model, in *Proceedings of 2020 IEEE International Conference on Robotics and Automation* (ICRA, 2020), pp. 9782–9788.
26. S. Yang, H. Chen, L. Zhang, Z. Cao, P. M. Wensing, Y. Liu, J. Pang, W. Zhang, Reachability-based push recovery for humanoid robots with variable-height inverted pendulum, in *Proceedings of 2021 IEEE International Conference on Robotics and Automation* (IEEE, 2021), pp. 3054–3060.
27. J. Liu, H. Chen, P. M. Wensing, W. Zhang, Instantaneous capture input for balancing the variable height inverted pendulum. *IEEE Robot. Autom. Lett.* **6**, 7421–7428 (2021).
28. Y. Zhao, L. Sentis, A three dimensional foot placement planner for locomotion in very rough terrains, in *Proceedings of 2012 12th IEEE-RAS International Conference on Humanoid Robots* (IEEE, 2012), pp. 726–733.
29. W. R. T. Roderick, M. R. Cutkosky, D. Lentink, Bird-inspired dynamic grasping and perching in arboreal environments. *Sci. Robot.* **6**, eabj7562 (2021).
30. R. Zufferey, J. Tormo-Barbero, D. Feliu-Talegón, S. R. Nekoo, J. Á. Acosta, A. Ollero, How ornithopters can perch autonomously on a branch. *Nat. Commun.* **13**, 7713 (2022).
31. L. Zheng, S. Hamaza, ALBERO: Agile landing on branches for environmental robotics operations. *IEEE Robot. Autom. Lett.* **9**, 2845–2852 (2024).
32. D. W. Haldane, M. M. Plecnik, J. K. Yim, R. S. Fearing, Robotic vertical jumping agility via series-elastic power modulation. *Sci. Robot.* **1**, eaag2048 (2016).
33. D. W. Haldane, J. K. Yim, R. S. Fearing, Repetitive extreme-acceleration (14-g) spatial jumping with Salto-1P, in *Proceedings of IEEE/RSJ International Conference on Intelligent Robots and Systems* (IEEE, 2017), pp. 3345–3351.
34. J. K. Yim, B. R. P. Singh, E. K. Wang, R. Featherstone, R. S. Fearing, Precision robotic leaping and landing using stance-phase balance. *IEEE Robot. Autom. Lett.* **5**, 3422–3429 (2020).
35. F. Saito, T. Fukuda, F. Arai, Swing and locomotion control for a two-link brachiation robot. *IEEE Control Syst. Mag.* **14**, 5–12 (1994).
36. A. L. Desbiens, A. T. Asbeck, M. R. Cutkosky, Landing, perching, and taking off from vertical surfaces. *Int. J. Robot. Res.* **30**, 355–370 (2011).
37. J. Moore, R. Cory, R. Tedrake, Robust post-stall perching with a simple fixed-wing glider using LQR-trees. *Bioinspir. Biomim.* **9**, 025013 (2014).
38. M. T. Pope, C. W. Kimes, H. Jiang, E. W. Hawkes, M. A. Estrada, C. F. Kerst, W. R. T. Roderick, A. K. Han, D. L. Christensen, M. R. Cutkosky, A multimodal robot for perching and climbing on vertical outdoor surfaces. *IEEE Trans. Robot.* **33**, 38–48 (2017).
39. G. A. Pratt, M. M. Williamson, Series elastic actuators, in *Proceedings of IEEE/RSJ International Conference on Intelligent Robots and Systems* (IEEE, 1995), pp. 399–406.
40. J. Thomas, J. Polin, K. Sreenath, V. Kumar, Avian-inspired grasping for quadrotor micro UAVs, in *Proceedings of International Design Engineering Technical Conference and Computers and Information in Engineering Conference* (ASME, 2013), pp. V06AT07A014.
41. W. Stewart, E. Ajanic, M. Müller, D. Floreano, How to swoop and grasp like a bird with a passive claw for a high-speed grasping. *IEEE/ASME Trans. Mechatron.* **27**, 3527–3535 (2022).
42. J. S. Lee, M. M. Plecnik, J. Yang, R. S. Fearing, Self-engaging spined gripper with dynamic penetration and release for steep jumps, in *Proceedings of IEEE International Conference on Robotics and Automation* (IEEE, 2018), pp. 6082–6089.
43. K. Nagaoka, H. Minote, M. Kyohei, Y. Shirai, K. Yoshida, T. Hakamada, H. Sawada, T. Kubota, Passive spine gripper for free-climbing robot in extreme terrain. *IEEE Robot. Autom. Lett.* **3**, 1765–1770 (2018).
44. C. E. Doyle, J. J. Bird, T. A. Isom, J. C. Kallman, D. F. Bareiss, D. J. Dunlop, R. J. King, J. J. Abbott, M. A. Minor, An avian-inspired passive mechanism for quadrotor perching. *IEEE/ASME Trans. Mechatron.* **2**, 506–517 (2012).
45. W. Crooks, S. Rozen-Levy, B. Trimmer, C. Rogers, W. Messner, Passive gripper inspired by *Manduca sexta* and the Fin Ray® effect. *Int. J. Adv. Robot. Syst.* **14**, 10.1177/1729881417721155 (2017).
46. D. Petković, N. D. Pavlović, Object grasping and lifting by passive compliant gripper, in *Mechanismentechnik in Ilmenau*, *Budapest und Niš: Technische Universität Ilmenau* (Universitätsverlag Ilmenau, 2012), pp. 55–64.
47. D. Petković, M. Issa, N. D. Pavlović, L. Zentner, Z. Ćojbašić, Adaptive neuro fuzzy controller for adaptive compliant robotic gripper. *Expert Syst. Appl.* **39**, 13295–13304 (2012).
48. T. Libby, T. Y. Moore, E. Chang-Siu, D. Li, D. J. Cohen, A. Jusufi, R. J. Full, Tail-assisted pitch control in lizards, robots and dinosaurs. *Nature* **481**, 181–184 (2012).

Acknowledgments

Funding: This work was supported by Army Research Office grant no. W911NF-18-1-0038 (J.K.Y., E.K.W., R.S.F., and R.J.F.), Army Research Office through a Multidisciplinary University Research 590 Initiatives (MURI) grant no. W911NF-1810327 (S.D.L. and R.J.F.), and NIH grant no. P20GM109090 (N.H.H.). **Author contributions:** Conceptualization: J.K.Y., E.K.W., S.D.L., N.H.H., R.J.F., and R.S.F. Discussion and interpretation: J.K.Y., E.K.W., S.D.L., N.H.H., R.J.F., and R.S.F. Data curation: E.K.W. and J.K.Y. Formal analysis: J.K.Y. Funding acquisition: R.S.F. and R.J.F. Experiments and data collection: E.K.W. Methodology: J.K.Y. and E.K.W. Project administration: R.S.F. and R.J.F. Resources: R.S.F. Software: J.K.Y. and E.K.W. Supervision: R.S.F. and R.J.F. Validation: S.D.L. Visualization: J.K.Y. and E.K.W. Writing—original draft: J.K.Y. and E.K.W. Writing—review and editing: J.K.Y., E.K.W., S.D.L., N.H.H., R.J.F., and R.S.F. **Competing interests:** The authors declare that they have no competing interests. **Data and materials availability:** All data needed to support the conclusions of this manuscript are included in the main text or Supplementary Materials. Data and corresponding processing code can be found at DOI 10.5061/dryad.xd2547dtf.

Submitted 1 July 2024
Accepted 19 February 2025
Published 19 March 2025
10.1126/scirobotics.adq1949

Science Robotics

Monopedal robot branch-to-branch leaping and landing inspired by squirrel balance control

Justin K. Yim, Eric K. Wang, Sebastian D. Lee, Nathaniel H. Hunt, Robert J. Full, and Ronald S. Fearing

Sci. Robot. **10** (100), eadq1949. DOI: 10.1126/scirobotics.adq1949

Science Robotics (ISSN 2470-9476) is published by the American Association for the Advancement of Science. 1200 New York Avenue NW, Washington, DC 20005. The title *Science Robotics* is a registered trademark of AAAS.